Since January 2020 Elsevier has created a COVID-19 resource centre with free information in English and Mandarin on the novel coronavirus COVID-19. The COVID-19 resource centre is hosted on Elsevier Connect, the company's public news and information website.

Carbohydrate Polymers 245 (2020) 116505

Contents lists available at ScienceDirect

Carbohydrate Polymers

journal homepage: www.elsevier.com/locate/carbpol

Chitin nanowhiskers from shrimp shell waste as green filler in acrylonitrile-butadiene rubber: Processing and performance properties

Midhun Dominic C.D.[a,b,*], Rani Joseph[c], P.M. Sabura Begum[b], Aswathy Raghunandanan[a], Nelwin T. Vackkachan[d], Dileep Padmanabhan[c], Krzysztof Formela[e,**]

[a] Department of Chemistry, Sacred Heart College (Autonomous), Kochi, Kerala, 682013, India
[b] Department of Applied Chemistry, Cochin University of Science and Technology (CUSAT), Kerala, 682022, India
[c] Department of Polymer Science and Rubber Technology, Cochin University of Science and Technology (CUSAT), Kerala, 682022, India
[d] Department of Chemistry, St. Albert's College (Autonomous), Kochi, Kerala, 682018, India
[e] Department of Polymer Technology, Faculty of Chemistry, Gdańsk University of Technology, Gabriela Narutowicza 11/12, 80–233, Gdańsk, Poland

ARTICLE INFO

Keywords:
Shrimp shell waste
Chitin nanowhisker
Acrylonitrile-butadiene rubber
Matrix-Filler interactions
Sustainable filler
Rubber nanocomposites

ABSTRACT

In this work, chitin nanowhiskers with high crystallinity index were obtained from shrimp shells waste using acid hydrolysis method and then comprehensively characterized. Subsequently, the impact of chitin nanowhisker content on processing and performance of acrylonitrile-butadiene rubber based nanocomposites was evaluated. The results showed that the addition of chitin nanowhiskers increased tensile strength and tear strength of nanocomposites by 116 % and 54 %, which was related to suitable dispersion of chitin nanowhiskers in matrix. Reinforcing effect of chitin nanowhiskers in acrylonitrile-butadiene rubber was also confirmed by Wolff activity coefficient, glass transition temperature and equilibrium swelling measurements. Moreover, it was found that higher content chitin nanowhiskers significantly improve the thermal stability of studied nanocomposites. The incorporation of chitin nanowhiskers resulted in increase of 74 °C for onset degradation temperature. This work confirmed that shrimp shell waste can be upcycled into chitin nanowhiskers – promising green filler in NBR for high-performance elastomeric applications.

1. Introduction

Acrylonitrile-butadiene rubber (NBR) is a synthetic, polar, special rubber, which found applications in the automotive, aerospace and petroleum industries (Tang & Zhang, 2014). NBR has excellent resistance to oil, chemicals, radiation and gas permeability and the properties of NBR can be easily modified by different acrylonitrile content (Fazli & Rodrigue, 2020). Even though NBR has excellent oil resistance its mechanical strength without the reinforcement phase is weak, because it does not crystallize under stress (Sadeghalvaad, Dabiri, Zahmatkesh, & Afsharimoghadam, 2019). For high-performance elastomeric applications of NBR, its mechanical strength should be improved. Reinforcing NBR with different nanofillers is a suitable method to enhance its performance properties.

It was reported that the addition of unmodified montmorillonite (Na-MMT) nanoclay into NBR significantly improve its modulus, tensile strength, thermal stability and glass transition temperature (Kader, Kim, Lee, & Nah, 2006). The dispersion of nano-$CaCO_3$ in NBR can be improved by the addition of the organoclay (Cloisite 30B) (Salkhord & Sadeghi Ghari, 2015). They found that the use of hybrid filler based on nano-$CaCO_3$ (10 phr) and Cloisite 30B (6 phr) provide an improvement in the dynamic mechanical, tensile and transport properties of NBR. Hu's group investigated the use of graphene oxide/halloysite nanotubes as hybrid fillers in NBR (Hu et al., 2020). They reported significant improvement of cross-link density, rubbery storage modulus and glass transition temperature of NBR based nanocomposites. The glass transition temperature of neat NBR increased from −19 °C to −11.5 °C by introducing 1 phr graphene oxide hybridized with nanosilica which shows the effectiveness of this hybrid filler system (Zhang, He, Wang, Rodrigues, & Zhang, 2018). Nanosilica was found to be a good reinforcing filler in NBR because of the hydrogen bonding interaction between the surface silanol groups of nanosilica and the nitrile group of NBR (Eyssa, Abulyazied, Abdulrahman, & Youssef, 2018).

After a thorough investigation of the literature, it was possible to

* Corresponding author at: Department of Chemistry, Sacred Heart College (Autonomous), Kochi, Kerala, 682013, India.
** Corresponding author at: Department of Polymer Technology, Faculty of Chemistry, Gdańsk University of Technology, Gabriela Narutowicza 11/12, 80–233, Gdańsk, Poland.
E-mail addresses: midhundominic@shcollege.ac.in (M. Dominic C.D.), krzysztof.formela@pg.edu.pl (K. Formela).

https://doi.org/10.1016/j.carbpol.2020.116505
Received 27 April 2020; Received in revised form 18 May 2020; Accepted 23 May 2020
Available online 02 June 2020
0144-8617/

observe that NBR rubber is mostly reinforced with fillers derived from non-renewable sources. Utilizing green fillers to improve the overall properties of NBR is hardly to find. Maria's group investigated the reinforcing effect of rice husk silica in NBR (Maria et al., 2017). They reported that the addition of rice husk silica in NBR improves the Payne effect, thermal stability, and compound viscosity considerably. Li et al. reported that the anti-skid properties and thermal stability of NBR were improved by the addition of biochar obtained from rice bran (Li, Zhang, & Cho, 2014). Abdul et al. reported that the addition of 2 phr nanocrystalline cellulose in NBR, improved the thermal stability and activation energy by 75 %, storage modulus by 12 GPa compared to virgin NBR (Abdul Rashid, Muhd Julkapli, & Abdul Hadi Yehya, 2018). Cotton linter derived cellulose nanocrystals in NBR showed excellent improvement in the tensile strength, modulus, and elongation at break at an optimum loading of 5 phr without altering the tear strength (Azman Mohammad Taib, Yeheye, & Muhd Julkapli, 2020)

Strong dependence on renewable resources has arisen as petroleum resources are limited. It has eventually led to the discovery and development of bio-based next-generation materials like nanocellulose and chitin nanowhiskers. Chitin, the second most abundant biopolymer is a polysaccharide with the molecular formula $(C_8H_{13}O_5N)_n$. It is a long-chain polymer of N-acetylglucosamine. Chitin is abundantly found in the exoskeleton of crab, mollusks, lobster, crayfish, shrimps, and krill etc. (Zhang & Rolandi, 2017). Recently, chitin was extracted from the guano of the bat *Rhinolophus hipposideros* (Kaya, Seyyar, Baran, & Turkes, 2014). Chitin was also extracted from fungi (Ekblad Alf, 1996) and corals (Bo et al., 2012). Based on the difference in the alignments of N-acetylglucosamine chains, they are classified into α (antiparallel chains with strong intermolecular interactions), β (parallel chains with weak intermolecular interactions) and γ (two chains going in the same direction and the other chain is antiparallel to them) (Alvarez, 2014). Chitin nanowhiskers have been emerging as a sustainable alternative for synthetic or petrochemical-based materials because of its unique properties like high modulus, stiffness, aspect ratio, strength, non-toxicity, anti-microbial action, biodegradability, crystallinity, biocompatibility, high binding energy and liquid-crystalline behaviour (Nge, Hori, Takemura, Ono, & Kimura, 2003). Due to these unique properties, chitin finds application in various fields such as food industry, the pharmaceutical industry, textile industry, paper industry, biomedical industry, cement industry, biosensing, drug delivery, etc. (Mincea, Negrulescu, & Ostafe, 2012). Chitin nanowhiskers can be prepared by acid hydrolysis (Lu, Weng, & Zhang, 2004), ultrasonication (Villa-Lerma et al., 2013), 2,2,6,6-tetramethylpiperidine-1-oxyl radical mediated oxidation (Fan, Saito, & Isogai, 2008), electrospinning method (Pillai & Sharma, 2009), mechanical treatment (Aklog et al., 2016), using ionic liquid (Kadokawa, Takegawa, Mine, & Prasad, 2011), fermentation process (Sini, Santhosh, & Mathew, 2007), etc.

Chitin nanowhiskers have a high longitudinal modulus of 150 GPa, which enables them to be used as reinforcements in different polymer matrices (Ofem, Anyandi, & Ene, 2017). Liu et al. studied the liquid-crystal behavior of chitin nanocrystals and it's reinforcing efficiency in natural rubber (Liu, Liu, Yang, Luo, & Zhou, 2018). They found that chitin nanocrystals forms a highly ordered network in natural rubber because of their capability to form inter and intramolecular hydrogen bonding. The authors also found that significant improvement in the mechanical properties and thermal stability was obtained by adding 10 wt% of chitin nanocrystals in natural rubber latex. A study conducted by Gopalan et al. revealed that chitin nanowhiskers derived from crab shells can form strong three dimensional networks in natural rubber latex, thereby improving overall mechanical properties of the resulting composite (Gopalan Nair & Dufresne, 2003). It was reported that β-chitin derived from squid pens, reinforced soy protein films show excellent tensile properties and water uptake resistance (Garrido, Etxabide, Caba, & Guerrero, 2017). Visakh et al. reported that the addition of crab shell chitin significantly increases the cure rate index and barrier properties of carboxylated styrene butadiene rubber (XSBR) (Visakh, Monti et al., 2012).

India especially the city Kochi ('Queen of Arabian Sea') is famous for its seafood export. It is estimated that the shellfish industry in India generates 60000 − 80000 tonnes of waste annually (Ravi Kumar, 2000). The shell waste produced in the pre-processing industry is a great threat because it creates disposal problems, pollution and health hazards (Biradar, Maladkar, & Kittur, 2016). Producing chitin from these shell waste is an effective strategy to overcome these problems. The foremost reason for choosing chitin is its abundant availability in these shell wastes and it remains one of the most underutilized organic polymers in nature's recipe book.

In the present study, we propose the preparation of chitin nanowhiskers (CHNW) from shrimp shell waste by the acid hydrolysis method. The prepared CHNW was comprehensively characterized using Fourier-transform infrared spectroscopy (FTIR), X-ray diffraction (XRD), transmission electron microscopy (TEM) and thermogravimetric analysis (TGA). Subsequently, novel nanocomposites based on acrylonitrile-butadiene rubber reinforced by various content of CHNW were developed and their cure characteristics, physico-mechanical, thermal, dynamic mechanical and transport properties were investigated. As far as we know, no attempts have been put forward so far to evaluate the reinforcing efficiency of chitin nanowhiskers in NBR, therefore the proposed study has several advantages. Preparation of chitin nanowhiskers from shrimp shell waste facilitates 'Blue Growth' (Boonstra, Valman, & Björkvik, 2018) in India which consists of many seafood exporting companies. This is a practical method to reduce the waste disposal and pollution problem associated with seafood exporting industries. The isolation of the value-added product chitin nanowhiskers from shrimp shell waste will generate additional revenue to seafood industries, which suffers a decline in their export due to current Coronavirus COVID-19 pandemic. The present work is a humble attempt to ensure environmental sustainability and to improve the environmental footprint in this highly industrialized global society.

2. Materials and methods

2.1. Materials

Shrimp shells were collected from the local market in Kochi, Kerala, India. Acrylonitrile-butadiene latex (34 % acrylonitrile content by mass) was supplied by Eliokem India Pvt. Ltd., Bombay. Acrylonitrile-butadiene rubber (KNB 35L) with 34 % acrylonitrile content was supplied by Kumho Petrochemicals Co., Ltd., South Korea. Zinc oxide was supplied by M/s Meta Zinc Ltd, Mumbai, India. Stearic acid was obtained from Godrej Soaps Pvt. Ltd, Mumbai, India. N-cyclohexyl-2-benzothiazole sulphenamide (CBS) was obtained from Merchem Ltd., Cochin, India. Tetramethylthiuram disulphide (TMTD) was supplied by Merchem Ltd., Cochin, India. Sulphur was obtained from Standard Chemicals Co. Pvt. Ltd., Chennai, India. Commercial antioxidant TQ (1,2-dihydro-2,2,4-trimethyl quinoline, polymerized) was obtained from Bayer India Ltd. Oxalic acid, hydrochloric acid, NaOH, H_2O_2, and $CaCl_2$ were supplied by Merck Specialities Pvt. Ltd., Mumbai, India.

2.2. Methods

2.2.1. Preparation of chitin nanowhisker (CHNW)

The shrimp shells were washed thoroughly with water several times and the washed shells were dried in an oven at 100 °C for 24 h.The dried shells were ground to a fine powder. About 100 g of the shrimp shell powder was refluxed with 2 N oxalic acid (1:10 g/mL) for 4 h. The acid is completely removed and the demineralised shrimp shell powder was subjected to bleaching. About 100 g the dried powder was stirred with 1000 mL 15 % hydrogen peroxide (v/v) and 100 mL 10 % NaOH solution. The bleaching process was repeated 2–3 times until the powder became white. After the bleaching, the chitin microfibers were thoroughly washed with distilled water. The obtained chitin fibers were

Table 1
Formulation for NBR-CHNW composites.

Sample Code	Solid NBR	Masterbatch		ZnO	Stearic acid	TQ	CBS	TMTD	S
		NBR latex	CHNW						
NBR -gum	50	50	–	4.5	2	1	1	0.25	2.5
NBR-CHNW2	50	50	2	4.5	2	1	1	0.25	2.5
NBR-CHNW4	50	50	4	4.5	2	1	1	0.25	2.5
NBR-CHNW6	50	50	6	4.5	2	1	1	0.25	2.5

refluxed with 3 N HCl (1:10 g/mL) for 2 h. The suspension was centrifuged and dialyzed in running water until the pH became 6. The suspension was subjected to homogenization in a D LAB homogenizer model D-500 for 30 min to get chitin nanowhisker.

2.2.2. Preparation of NBR-CHNW composites

NBR-CHNW composites were prepared in a two-step process. First step involves the masterbatch preparation in NBR latex followed by compounding the masterbatch with solid NBR and vulcanizing agents using two-roll mills. A good dispersion of CHNW in NBR latex (37 % dry rubber content) was obtained by mixing the suitable amount of CHNW in NBR latex for 3 h. The dispersion is coagulated using 0.5 % $CaCl_2$ solution. The obtained sheet was oven dried at 70 °C for 48 h. CHNW loadings were adjusted to get 2, 4, 6 phr nanowhisker in the final composites. In the second step, the compounding of the masterbatch with solid NBR and other vulcanizing agents was carried out using two-roll mills. Chitin nanowhiskers were oriented in the mills direction by passing through the tight gap in the mills at the end of the mixing process. The formulation for preparing NBR-CHNW composites is given in Table 1. Vulcanization of various test samples was carried out in an electrically heated hydraulic press having 45 cm × 45 cm platen at 160 °C at a pressure of 2844 psi on the mould up to optimum cure time. Cured NBR-CHNW composites were conditioned for 24 h.

2.2.3. Characterization

The cure characteristics of the prepared NBR-CHNW composites were determined by using Rubber Process Analyser, RPA 2000 as per ASTM D 5289. The stress-strain tests were carried on a Shimadzu Model AGI Universal Testing Machine as per ASTM D 412. Tear resistance of the samples was tested as per ASTM D 624. The hardness of samples was measured as per ASTM D 2240 by shore A type Durometer. The abrasion resistance was performed using Bariess DIN abrader, Germany (ASTM D 5963). Compression set was studied on a compression set apparatus as per ASTM D 395 with a spacer thickness 9.5 mm. Fourier-transform infrared analysis (FTIR) was conducted on Thermo Nicolet, Avatar 370 model IR spectrometer, in 4000-400 cm^{-1} spectral range with a resolution of 4 cm^{-1}. Thermogravimetric analysis was performed on thermogravimetric analyzer Q-50, TA instruments with a heating rate of 20 °C/min under nitrogen atmosphere. The fracture surfaces of the vulcanized samples were studied with JEOL JSM 8390 L V scanning microscope. TEM imaging was done using JEOL JEM 2100 High resolution transmission electron microscope. XRD analysis was conducted using Bruker AXS D8 Advance X-Ray powder diffractometer.

Swelling behavior and cross-link density of NBR-CHNW nanocomposites were determined by equilibrium swelling method (Dominic, Joseph, Begum et al., 2020) and the solvent used was toluene. Mol % uptake (Q_t) of solvent for the samples was calculated using Eq. (1):

$$Q_t = \left(\frac{(W_S - W_i)/M_s}{W_i} \right) \times 100\% \quad (1)$$

Where W_s is the weight of the swollen sample and W_i the initial weight of the sample i.e. the weight of the sample before swelling, M_s the molar mass of solvent.

Swelling index was calculated using the following Eq. (2):

$$Swellingindex = \frac{W_s - W_i}{W_i} \quad (2)$$

Where W_s is the weight of the swollen sample and W_i the initial weight of the sample i.e. the weight of the sample before swelling.

Cross-link density (ν) was calculated according to Eq. (3):

$$\nu = \frac{1}{2M_c} \quad (3)$$

Where M_c is the molecular mass between successive cross-links. M_c is given by the Flory-Rehner Eq. (4) (Flory & Rehner, 1943):

$$M_c = \frac{-\rho_r V_s V_r^{1/3}}{\ln(1 - V_r) + V_r + \chi V_r^2} \quad (4)$$

Where ρ_r is the density of rubber, V_s the molar volume of the solvent, χ the rubber solvent interaction parameter and V_r the volume fraction of swollen rubber which was calculated using Ellis and Welding Eq. (5) (Bryan & Welding, 1964):

$$V_r = \frac{(d - fw)\rho_r^{-1}}{(d - fw)\rho_r^{-1} + A_s\rho_s^{-1}} \quad (5)$$

Where d is the deswollen weight of the polymer, f the volume fraction of insoluble components, w is the initial weight of the polymer, $A_s$the amount of solvent absorbed and ρ_s density of the solvent. χ is determined using Hildebrand Eq. (6):

$$\chi = \beta + \frac{V_s(\delta_s - \delta_p)^2}{RT} \quad (6)$$

Where β is the lattice constant, R the universal gas constant, T the absolute temperature, δ_s and δ_p are solubility parameters of the solvent and polymer respectively.

TA Instruments DMA Q800 Dynamic mechanical analyser was used to measure dynamic mechanical properties of the samples in tension mode. Samples for DMA measurement were cut from the vulcanized sheets, having the dimension 30 mm × 3 mm × 2 mm. For the temperature sweep analysis, the samples were tested from −40 to 80 °C at a ramp rate of 3 °C/min and a frequency of 1 Hz.

The amount of polymer chains immobilized through matrix-filler interactions is determined by using Eq. (7) (Formela, Hejna, Piszczyk, Saeb, & Colom, 2016):

$$C_v = 1 - (1 - C_0)\frac{W}{W_0} \quad (7)$$

Where C_v is the volume fraction of the immobilized polymer chains, C_0 stands for the volume fraction of the immobilized polymer chains in the pure acrylonitrile-butadiene rubber (taken to be zero), and W and W_0 are energy loss fraction for NBR-CHNW composite and pure NBR, respectively. Energy loss fractions W can be calculated from the tan δ in accordance to Eq. (8):

$$W = \frac{\pi\tan\delta}{\pi\tan\delta + 1} \quad (8)$$

For better understanding the interfacial interactions between NBR and CHNW, the adhesion factor (A) was calculated from the loss factor (tan δ) using Eq. (9) (Formela et al., 2016):

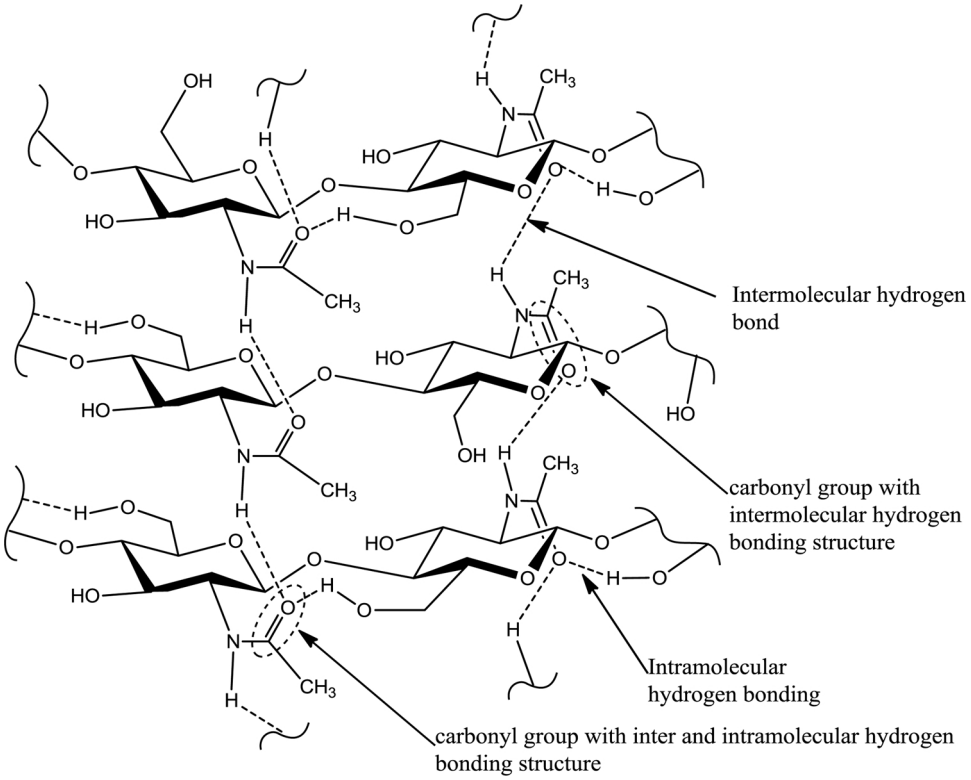

Fig. 1. Inter and intramolecular hydrogen bonding interaction in chitin nanowhiskers.

$$\frac{\tan \delta_c}{\tan \delta_m} \cong (1 - V_f)(1 + |A) \quad (9)$$

Where, V_f is the volume fraction of the filler phase, tan δ_C the loss tangent of NBR-CHNW composite and tan δ_m the loss tangent of pure NBR.

3. Results and discussion

3.1. Fourier-transform infrared spectroscopy (FTIR)

The inter and intramolecular hydrogen bonding interaction in chitin nanowhiskers is shown in Fig. 1. The FTIR spectroscopy was found to be very useful to distinguish the three crystalline polymorphs of CHNW (α, β, and γ) and its molecular interactions. The FTIR spectrum of the obtained chitin nanowhiskers was shown in Fig. 2A. Generally, chitin shows absorption bands around 1660, 1550, 973 cm^{-1} which are labelled as amide I, II and III bands (Jang, Kong, Jeong, Lee, & Nah, 2004). Literature shows that for α-chitin, two separate absorbance bands are observed at 1656 and 1622 cm^{-1} (Jang et al., 2004). The band at 1656 cm^{-1}, corresponds to the intermolecular hydrogen bonding (−CO···HN) and the band at 1622 cm^{-1} indicates the intramolecular hydrogen bonding (−CO···$HOCH_2$) (Jang et al., 2004). For β-chitin, only one absorption band is observed at 1659 cm^{-1} which corresponds to the stretching of C−O group (amide I) hydrogen-bonded to amide II (−NH)−.The FTIR spectral analysis of the prepared CHNW showed that the amide I absorption band splits into two, and the bands were observed at 1656 and 1622 cm^{-1}. This reveals that α-form is present in the prepared CHNW. The bands at 3457 cm^{-1} and 3261 cm^{-1} correspond to the −OH stretching and N−H stretching respectively. The band at 1656 cm^{-1} corresponds to the amide I stretching of CO═, while the band at 1553 cm^{-1} corresponds to the stretching or NH− deformation of amide II, and bands at 1375 cm^{-1} and 897 cm^{-1} correspond to the symmetrical deformation of amide III (Kaya et al., 2014).

3.2. X-ray diffraction (XRD)

The XRD pattern of the prepared CHNW was shown in Fig. 2B. The XRD analysis was conducted to determine the structure, phase purity and degree of crystallinity of the prepared CHNW. The relative intensity of CHNW showed peaks at 2θ = 9.3°, 12.7°, 19.4°, 20.7°, 23.4°, and 26.3° correspond to the reflections from the plane (020), (021), (110), (120), (130), (013) respectively. These peaks are characteristic of α-chitin (Kaya et al., 2014). The crystallinity index (*CI*) of CHNW was determined using the Eq. (10) (Kaya et al., 2014):

$$CI = \frac{I_{110} - I_{am}}{I_{110}} \times 100 \quad (10)$$

Where I_{110} is the highest intensity at 2θ = 20° and I_{am} the amorphous diffraction intensity at 2θ = 13°. The *CI* of the prepared CHNW was found to be 86 %. The *CI* of CHNW was higher than that of *CI* of chitin nanofibers obtained from fungi and resting eggs (Wysokowski et al., 2013). The high crystallinity index of CHNW was due to the removal of amorphous regions and proteins from chitin powder, which shows the effectiveness of the chemical treatment employed for the isolation of CHNW.

3.3. Transmission electron microscopy (TEM)

TEM image of the synthesized CHNW was shown in Fig. 2C. The CHNW showed rod-like morphology and the whiskers were in the nanometer range. The diameter of the individual fragments of CHNW ranges between 25 − 32 nm. The length of the prepared nanowhiskers was in the range of 400 nm. The aspect ratio (L/D) of CHNW was found to be in the range 12 − 16. The aspect ratio of the prepared CHNW was similar to the aspect ratio of chitin nanowhiskers prepared from crab shells (L/D = 15) and less than that from *Riftia* tubes (L/D = 120) by the HCl hydrolysis method (Mincea et al., 2012). The TEM image also shows that the prepared whiskers are highly agglomerated because of inter and intramolecular hydrogen bonding present in them.

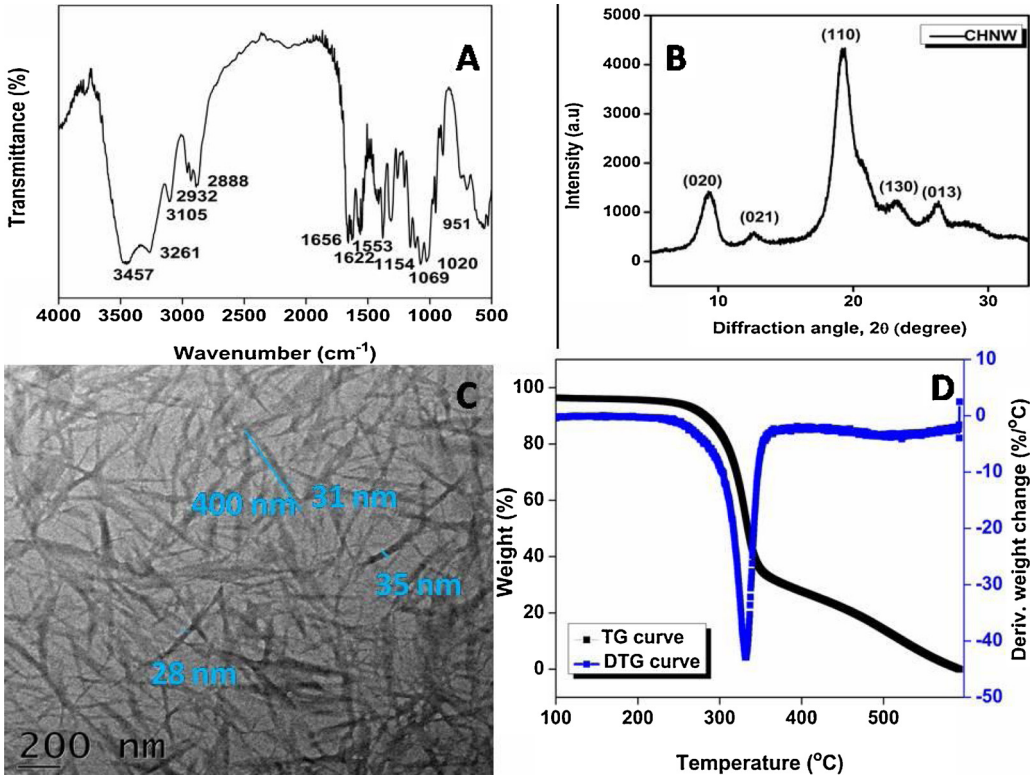

Fig. 2. (A) FTIR spectra, (B) XRD pattern, (C) TEM image and (D) TGA and DTG curves of CHNW.

3.4. Thermogravimetric analysis of CHNW

Thermogravimetric (TGA) and derivative thermogravimetric (DTG) curves of the prepared CHNW were plotted in Fig. 2D. The curves showed that the thermal decomposition of CHNW takes place in a single step and it happens between 275 – 460 °C. The onset degradation temperature (T_{on}) of the synthesized CHNW was found to be at 277 °C. The temperature at which 50 % degradation of CHNW occurs (T_{50}) at 335 °C. From the DTG curve, the temperature at which maximum degradation of CHNW occurs (T_{max}) at 332 °C. The residue at 500 °C of CHNW was around 14 %. The T_{50}, T_{max} and residue content values indicate that the thermal stability of the prepared chitin nanowhiskers was less than that of regenerated chitin from alkaline/urea aqueous system (Yu, He, Luo, Jia, & Dufresne, 2017). On the other hand, the crystallinity index of the prepared CHNW (86 %) was found to be higher than that of the regenerated chitin (76.3 %).

3.5. Cure characteristics of NBR-CHNW composites

Table 2 shows the cure characteristics of NBR-CHNW composites. Optimum cure time means the time required for 90 % vulcanization. The cure analysis shows that the optimum cure time (t_{90}) of CHNW loaded nanocomposites is higher than NBR gum. The increase in t_{90} value of NBR-CHNW composites may be due to the absorption of accelerators on the active surfaces of CHNW thereby delaying the curing process. The scorch was found to be increased with an increase in CHNW loading ascribed to the adequate scorch safety to the prepared composites. The decrease in the cure rate index value of the prepared NBR-CHNW composites showed that CHNW cannot impart an activating effect in the curing reaction of NBR. Balachandran et al. reported an activating effect in the cure reaction of NBR when nano-calcium carbonate was used as a filler (Balachandran & Bhagawan, 2012). Differential torque is a measure of the extent of the cross-link formation and interaction between NBR & CHNW (De, Kr.Panda, Roy, Bhunia, & Ismail Jaman, 2012). The differential torque was found to be maximum for the NBR-CHNW2 composite ascribed to its high cross-link density. The increase in the differential torque of the prepared nanocomposites was due to the entanglement of nitrile rubber chains by chitin nanowhiskers. The Wolff activity coefficient (α_F) corresponds to the the reinforcement effect of the CHNW in NBR. Higher the value of α_F, higher will be the reinforcement effect of the CHNW. Consider the following Eq. (11):

$$\frac{\Delta M_x}{\Delta M_0} - 1 = \alpha_F \frac{m_x}{m_p} \tag{11}$$

Where ΔM_x is the torque increment of NBR-CHNW composites in dNm, ΔM_0 the torque increment of NBR gum in dNm, m_x the weight of filler and m_p the weight of the polymer.The values of α_F were found to be

Table 2
Curing parameters and Wolff activity coefficient determined for NBR-CHNW nanocomposites.

Properties	NBR- gum	NBR-CHNW2	NBR-CHNW4	NBR-CHNW6
Scorch time, t_{s2}(min)	2.08	2.56	3.03	3.21
Optimum cure time, t_{90}(min)	5.06	5.55	6.04	7.29
Cure rate index (min^{-1})	33.55	33.44	33.22	24.50
Minimum torque(M_L, dNm)	0.46	0.65	0.66	0.70
Maximum torque(M_H, dNm)	7.34	7.77	7.67	7.61
Differential torque, $M_H - M_L$ (dNm)	6.88	7.12	7.01	6.91
Wolff activity coefficient	–	1.74	0.47	0.07

Table 3
Physico-mechanical and sorption parameters of NBR − CHNW composites.

Properties	NBR	NBR-CHNW2	NBR-CHNW4	NBR-CHNW6
Tensile strength (MPa)	2.75 ± 0.25	5.95 ± 0.67	5.02 ± 0.89	4.69 ± 0.37
Modulus at 300 % elongation (MPa)	1.95 ± 0.20	4.27 ± 0.49	4.71 ± 0.38	5.87 ± 0.25
Elongation at break (%)	395 ± 15	354 ± 11	363 ± 12	371 ± 14
Tear strength (N/mm)	19.76 ± 0.75	24.85 ± 0.61	28.98 ± 0.69	31.25 ± 0.67
Hardness (Shore A)	45 ± 1	48 ± 1	51 ± 1	53 ± 1
Compression set (%)	10.23 ± 0.25	18.43 ± 0.25	14.38 ± 0.29	15.75 ± 0.25
Abrasion resistance index (ARI)	180 ± 5	192 ± 3	186 ± 4	183 ± 5
Swelling index (%)	207 ± 2	204 ± 1	205 ± 1	209 ± 2
Cross-link density(mol/g × 10^{-4})	1.31 ± 0.05	1.38 ± 0.03	1.34 ± 0.05	1.29 ± 0.06

positive for all the prepared NBR-CHNW composites. Maximum value of α_F was found to be at 2 phr CHNW addition owing to the better reinforcing effect of CHNW in NBR.

3.6. Physico-mechanical properties of NBR-CHNW nanocomposites

The tensile properties of NBR-CHNW nanocomposites are listed in Table 3. The tensile strength of NBR gum, NBR-CHNW2, NBR-CHNW4, NBR-CHNW6 composites was found to be 2.75 ± 0.25 MPa, 5.95 ± 0.67 MPa, 5.02 ± 0.89 MPa and 4.69 ± 0.37 MPa, respectively. The tensile strength of CHNW incorporated NBR showed improved tensile strength compared to neat NBR. About 116 % improvement in tensile strength was observed in the NBR-CHNW2 composite compared to NBR gum. This is the major achievement of the present technique employed. By applying latex stage processing, the chitin nanowhiskers will be more dispersed (evident from fractographic studies) in the NBR matrix compared to conventional mixing. Stress transfer theory can be applied to explain the reinforcement of CHNW in NBR. When the nanowhiskers were aligned in the direction of strain, they could effectively transfer the stress from the matrix and can also prevent the propagation of microcracks (Tian et al., 2011). The hydrogen bonding interaction between the −OH groups of CHNW and nitrile group of NBR rubber at the interface, the three-dimensional intra and inter hydrogen bonding networks between the chitin nanowhiskers, uniform dispersion and high aspect ratio of chitin nanowhiskers might be responsible for the significant improvement in the tensile strength of NBR-CHNW nanocomposites. The schematic representation of the possible mechanism of interaction between CHNW and NBR was given in Fig. 3. It was observed that the tensile strength of the prepared NBR nanocomposites decreased after 2 phr CHNW addition. At high CHNW loading, agglomeration of nanowhiskers resulted in the formation of bundles. In this case, the filler-filler interaction over ways matrix-filler interactions. Then nanowhiskers would be debonded at the interface creating voids. These voids may act as stress concentration centers that might be responsible for the deterioration of tensile strength at high CHNW loading. The elongation at break of NBR gum, NBR-CHNW2, NBR-CHNW4 and NBR-CHNW6 composites was found to be 395 ± 15 %, 354 ± 11 %, 363 ± 12 %, 371 ± 14 %, respectively. The elongation at break of NBR-CHNW composites was found to be less than NBR gum. The decrease in the elongation at break of NBR-CHNW nanocomposites was due to the immobilization of the polymer chains by the CHNW network. The low value of elongation at break of NBR-CHNW2 composite ascribed to the high interfacial interaction and high cross-link density. Boonbumrung reported a similar trend in tensile strength and elongation at break when multiwalled carbon nanotubes have used as a filler in NBR (Boonbumrung, Sae-oui, & Sirisinha, 2016).

The modulus at 300 % elongation of NBR gum, NBR-CHNW2, NBR-CHNW4 and NBR-CHNW6 composites were found to be 1.95 ± 0.20 MPa, 4.27 ± 0.49 MPa, 4.71 ± 0.38 MPa and 5.87 ± 0.25 MPa respectively. The modulus at 300 % elongation of the prepared composites was found to be increased with an increase in the concentration of chitin nanowhiskers owing to the interfacial compatibility and reinforcing efficiency of CHNW. The tear strength of NBR gum, NBR-CHNW2, NBR-CHNW4 and NBR-CHNW6 composites was 19.76 ± 0.75 N/mm, 24.85 ± 0.61 N/mm, 28.98 ± 0.69 N/mm and 31.25 ± 0.67 N/mm respectively. The NBR-CHNW6 composite showed a significant improvement of 58 % in tear strength compared to neat NBR. The increase in tear strength along the longitudinal direction was due to the obstruction created to the tear path by chitin nanowhiskers. Even though the tensile strength was found to be highest at 2 phr CHNW loading, the tear strength was found to be maximum at 6 phr filler loading. Dominic, Joseph, Begum et al. reported a similar trend when cellulosic nanofibers isolated from the parasitic plant *Cuscuta reflexa* were used as a filler in natural rubber (Dominic, Joseph, Begum et al., 2020).

The hardness of NBR-CHNW nanocomposites increased with an

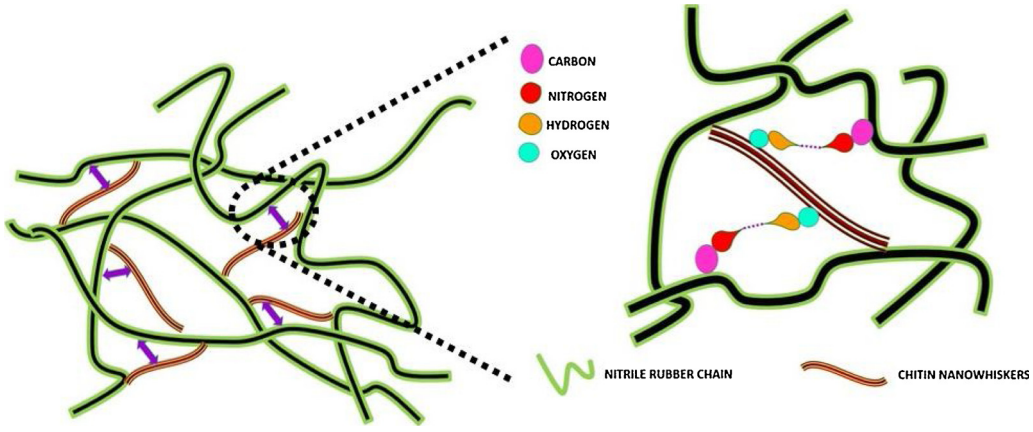

Fig. 3. Schematic representation of the possible interaction between NBR and CHNW.

increase in CHNW loading due to the improved rigidity of the composites. The hardness (Shore A) of NBR gum increased from 45 to 53 by the addition of 6 phr CHNW. The abrasion resistance index (ARI) was found to be maximum for NBR-CHNW2 composite. The effective interaction between the nanowhiskers and the matrix prevents the scooping of the material as chunks by the abrader. The high ARI value of the prepared nanocomposites indicates a longer service life. The compression set value was found to be minimum for NBR-CHNW2 composite compared to other vulcanizates ascribed to the low residual deformation, higher cross-link density and better rubber-nanowhisker interactions (Rattanasom, Saowapark, & Deeprasertkul, 2007).

3.7. Swelling studies of NBR-CHNW nanocomposites

The sorption parameters of NBR-CHNW composites are listed in Table 3. The molecular transport of solvent molecules across NBR is a kinetic parameter that is mainly influenced by the free volume present in the material, the segmental mobility of NBR chains, cross-link density and the nature of the penetrant molecules. The swelling studies of the prepared NBR nanocomposites were conducted to gather valuable information about the strength of interface, 3D-network formation, the degree of dispersion of CHNW in the rubber matrix (Prasanth Kumar, Getthakumari Amma, & Sabu, 1995). The plot of mol % uptake (Q_t) vs. time$^{1/2}$ of NBR gum and NBR-CHNW composites were shown in Fig. 4A. The swelling index of NBR gum, NBR-CHNW2, NBR-CHNW4 and NBR-CHNW6 were found to be 207 ± 2, 204 ± 1, 205 ± 1, 209 ± 2, respectively. The lowest swelling index value was reported for NBR-CHNW2 composite. It was observed that no significant difference in the swelling index values of NBR-CHNW2 and NBR-CHNW4 nanocomposites. The decrease in the swelling index values of NBR nanocomposites except for NBR-CHNW6 compared to NBR gum was might be due to the decrease in the availability of free volume in the material which arises from the strong interfacial adhesion between CHNW and the polymer matrix. The uniform dispersion and the tangling effect of CHNW restrict the anisotropic swelling of the composites. The robust complex network structure created by the filler-filler and matrix-filler interactions may hinder the entry of solvent molecules to the matrix owing to the decrease in the swelling index of the material. The formation of CHNW network reduces the volume swell of the rubber phase, owing to the decrease in permeation of the solvent to the bulk (Yu et al., 2017). The polarity and tortuosity of CHNW resist the entry of non-polar solvent molecules into the NBR matrix. The three-dimensional networks of CHNW act as entanglements or physical cross-links of elastomers. This restricts the segmental motion of rubber chains and the movement of the penetrant molecule between the polymer chains. An increase in the swelling index at higher CHNW loading (6 phr) was due to the agglomeration of nanowhiskers. The cross-link density(mol/g$\times 10^{-4}$) of pure NBR, NBR-CHNW2, NBR-CHNW4 and NBR-CHNW6 composite were found to be 1.31 ± 0.05, 1.38 ± 0.03, 1.34 ± 0.05, 1.29 ± 0.06, respectively. The hydrogen bond interaction between CHNW and NBR increases the cross-link density. The cross-link density has reached a maximum value at 2 phr CHNW addition, owing to the rigidity of the composite. Boonbumrung's group observed similar improvement in cross-link density when multiwalled carbon nanotube and precipitated silica were used as fillers in NBR (Boonbumrung et al., 2016). The cross-link density was found to be decreased at 6 phr CHNW loading due to the steric hindrance created by CHNW between the molecular chains of NBR. At 6 phr CHNW loading, the increase in the number of intramolecular hydrogen bonds within CHNW may result in reduced matrix-filler interaction, leading to a detrimental effect in cross-link density. It can be related with the dispersion issue at 6 phr CHNW loading. The cross-link density measurements were in line with the differential torque values reported for the prepared composites.

3.8. Thermogravimetric analysis of NBR-CHNW composites

The TGA curves of neat NBR and NBR-CHNW composites were shown in Fig. 4B. All the prepared composites showed single-stage degradation behavior similar to the one reported previously (Balachandran & Bhagawan, 2012). The initial weight loss around 80 °C–100 °C was due to the evaporation of moisture from the sample. The main degradation occurs between 250 and 400 °C in all the samples was due to the chain scission and cross-link breakage. The onset degradation temperature (T_{on}) of NBR gum, NBR-CHNW2, NBR-CHNW4, and NBR-CHNW6 was found to be 300 °C, 318 °C, 354 °C, and 374 °C, respectively. Eyssa et al. reported an increase in 57 °C on the onset degradation temperature of NBR by incorporating 20 phr silica (Eyssa, Abulyazied, Abdulrahman, & Youssef, 2017). By the addition of 6 phr CHNW, T_{on} increased to 74 °C compared to neat NBR. This indicates the effectiveness of CHNW in delaying the thermal degradation of NBR. The decomposition of CHNW results in the formation of volatiles and char. These residues act as a protective barrier to both mass and energy from the burning surface to the attached polymeric chains. The decreased mobility of the NBR phase in the proximity of CHNW results in slower diffusion of degradation products from the material. The temperature at which 50 % degradation occurs (T_{50}) for the NBR gum, NBR-CHNW2, NBR-CHNW4 and NBR-CHNW6 composite was found to be 450 °C, 454 °C, 460 °C and 466 °C respectively. The thermal analysis explicitly clarifies that there is a remarkable improvement in T_{50} of NBR by the addition of chitin nanowhiskers. The increase in the thermal stability of CHNW reinforced NBR composites is associated with the restricted mobility of rubber chains generated by the rigid network of chitin nanowhiskers (Liu et al., 2018). The strong interfacial interaction between CHNW and NBR was also responsible for the improved thermal stability of the nanocomposite. The 'imprisonment' of rubber chains in the rigid three-dimensional hydrogen-bonded network substantially improve the

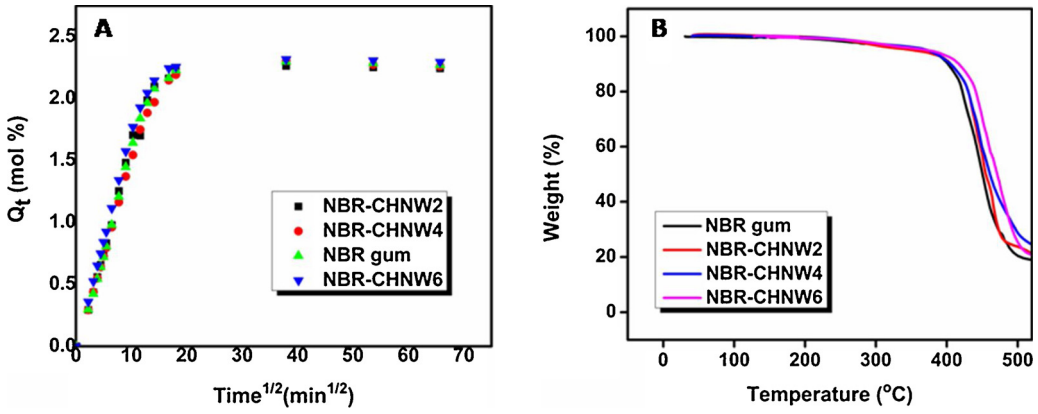

Fig. 4. (A) Mol % uptake (Q_t) vs. time$^{1/2}$ of NBR gum and NBR-CHNW composites and (B) thermogravimetric curves of NBR gum and NBR-CHNW nanocomposites.

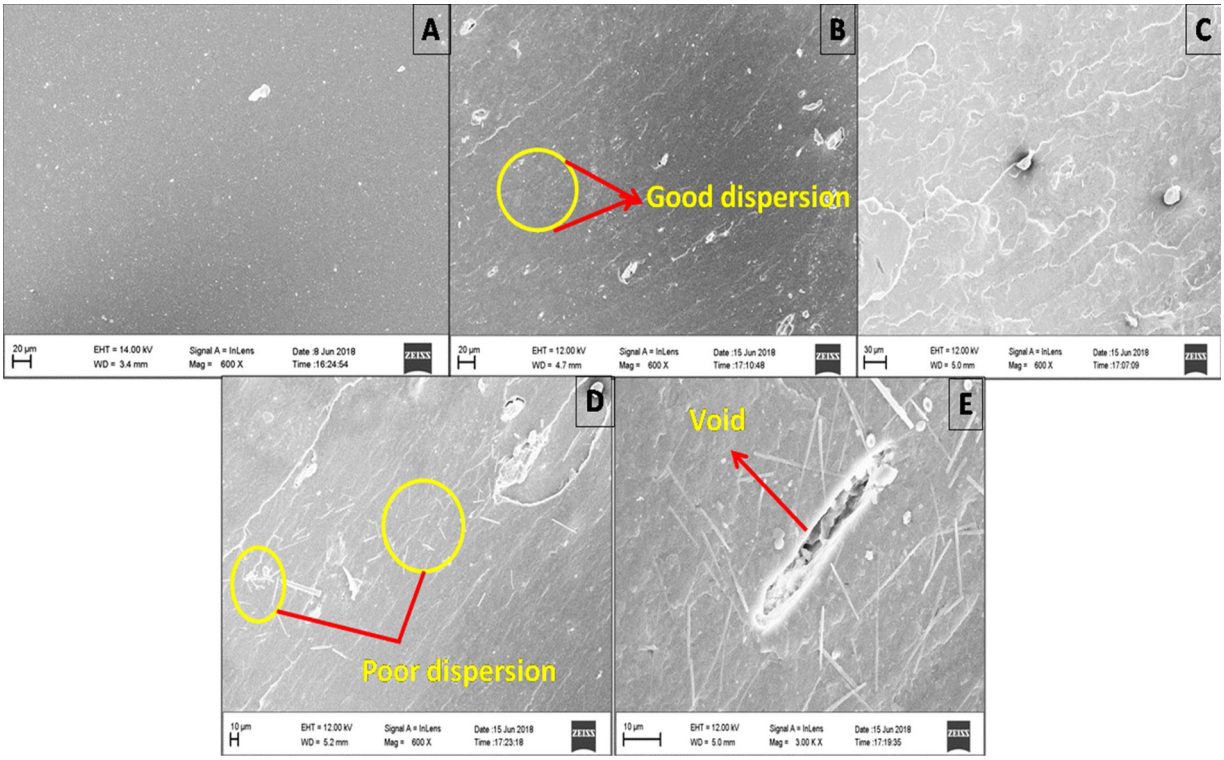

Fig. 5. SEM images of tensile fractured samples of vulcanizates (A) NBR gum (B) NBR-CHNW2, (C) NBR-CHNW4, (D) & (E) NBR-CHNW6 under two different magnifications (600X and 300000X).

cross-link density and rigidity of the matrix, ascribed to the better thermal stability of the composites prepared. The uniform dispersion of CHNW in NBR hinders the permeability of volatile decomposition products out of the material, slow down the pace of degradation of the composites (Visakh, Thomas, Oksman, & Mathew, 2012). The high crystallinity index of the synthesized chitin nanowhiskers may also play a key role in improving the thermal stability of the composites. The residue at 500 °C of NBR gum, NBR-CHNW2, NBR-CHNW4, NBR-CHNW6 composites was found to be 17.53 %, 23.72 %, 25.42 % and 28.07 %, respectively. It was observed that the residue content at 500 °C of NBR-CHNW composites increased with an increase in CHNW concentration. This suggests that chitin nanowhiskers were successfully introduced into NBR and these nanowhiskers improved the thermal stability of the composites considerably.

3.9. Fractographic studies of NBR-CHNW nanocomposites

The fractured surface of NBR gum seems to be smooth and cryogenic (Fig. 5A). As CHNW loading increases the surface became irregular and rough. This shows plastic deformation and a fracture mechanism transition. The dispersion of CHNW in the NBR matrix is critical for the ultimate mechanical properties of the prepared composites (Hu et al., 2020). The SEM image of the tensile fractured specimen of NBR-CHNW2 (Fig. 5B) composite showed that chitin nanowhiskers were distributed in the polymer matrix homogeneously. No voids and aggregates of CHNW were seen in the sample. This indicates good compatibility between NBR and CHNW at low filler loading. The roughness, undulations and craters are seen in the tensile fractured surface of NBR-CHNW2 (Fig. 5B) and NBR-CHNW4 composite (Fig. 5C) specify better filler-matrix interaction and effective stress transfer. The ridged surface which is an evidence of good mechanical properties seen in the fractured specimen of NBR-CHNW2 and NBR-CHNW4 was similar to the one reported by Zhong et al. (2018). Fig. 5D shows aggregates of CHNW, indicate the non-uniform distribution of chitin nanowhiskers in NBR at 6 phr CHNW loading. Clear phase separation and defects were observed at higher CHNW loading (Fig. 5E). The debonding and pullout of chitin nanowhiskers creates voids which results in the failure of the composite. These voids act as nuclei for crack propagation, which will ultimately result in inferior mechanical properties (Sae-Oui, Rakdee, & Thanmathorn, 2002).

3.10. Dynamic mechanical analysis (DMA)

The dynamic mechanical analysis was conducted to investigate the viscoelastic properties and the interaction between CHNW and NBR. Fig. 6 shows the curves of the storage modulus (Fig. 6A), loss modulus (Fig. 6B) and the loss tangent (Fig. 6C) of NBR, NBR-CHNW2, NBR-CHNW6 composites as a function of temperature at a frequency of 1 Hz. In the glassy region, the storage modulus at −40 °C was found to be higher for NBR-CHNW2 composite (1473 MPa) compared to NBR gum (1189 MPa) and NBR-CHNW6 (1384 MPa). The enhanced storage modulus of the prepared NBR nanocomposites even below the glass transition temperature showed the reinforcing efficiency of CHNW in NBR (Zhang et al., 2014). At around −25 °C a sharp decrease in storage modulus was observed for all the prepared nanocomposites. This might be due to the energy dissipation process happens in all the prepared NBR composites. It was observed that at high temperature (T > glass transition temperature) the storage modulus was found to be almost constant and a plateau was reached (rubbery region). The storage modulus at 25 °C (rubbery modulus) of NBR, NBR-CHNW2 and NBR-CHNW6 composites were found to be 3.651, 6.157 and 5.968 MPa respectively. About 68 % improvement in the rubbery modulus was achieved by the addition of 2 phr CHNW in the NBR matrix. The degree of crystallinity of the material is a crucial factor that influences the rubbery modulus (Gopalan Nair & Dufresne, 2003). The crystalline domains of chitin nanowhiskers act as physical cross-links for the NBR chains. Chen et al. reported similar improvements in the rubbery modulus when NBR foam is reinforced with cellulose nanocrystals (Chen, Zhang, Xu, & Cao, 2015). The chitin nanowhiskers can interact with NBR in two ways. The first way is by forming hydrogen bonds with

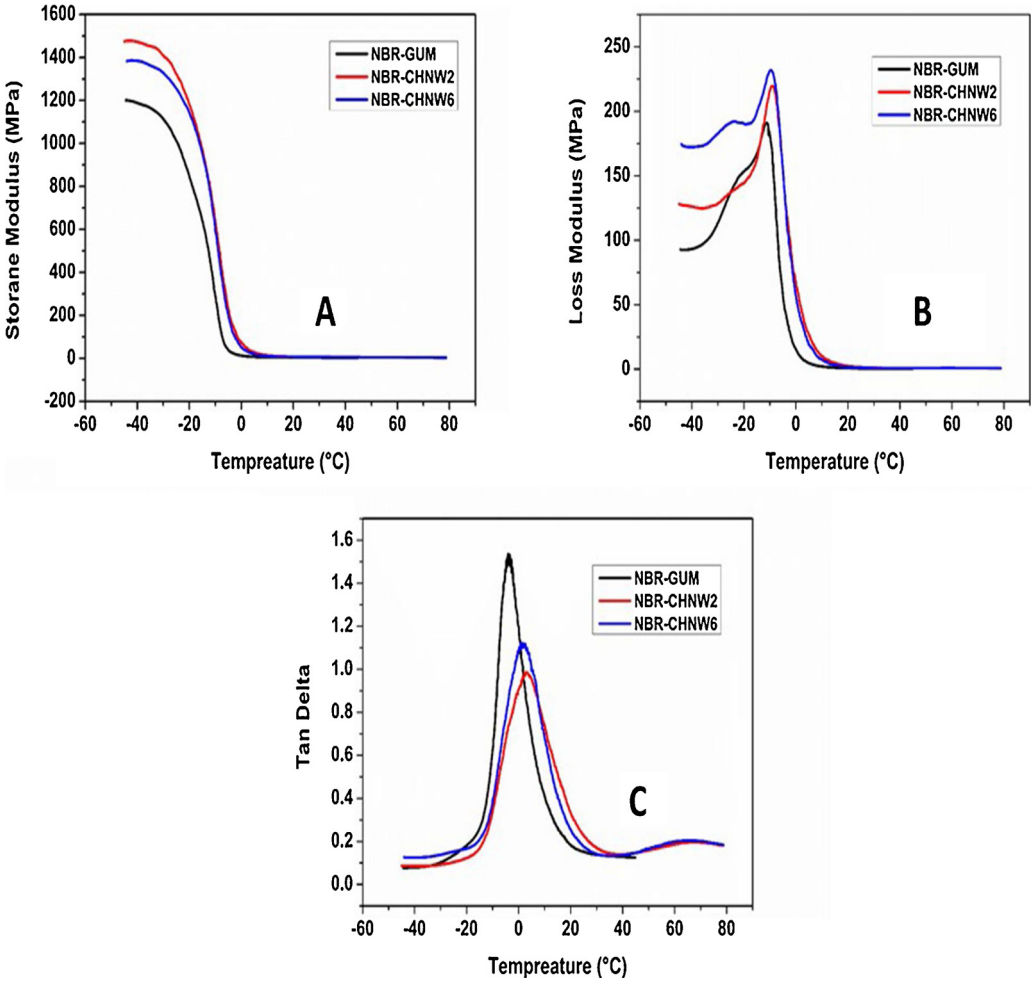

Fig. 6. Storage modulus, loss modulus and tanδ of NBR-CHNW nanocomposites.

the nitrile group of NBR and −OH groups of CHNW. Secondly, CHNW can interacts with chains of NBR because of its nano-size effect forming 'restrict rubber' (Chen et al., 2015). The effective hydrogen bonding interaction between CHNW and NBR at the interface boundary and the 3D-networks of CHNW (due to inter and intramolecular hydrogen bonding) provide improved wetting by polymer chains which also may be the reason for the improvement in storage modulus. The high value of storage modulus at 2 phr CHNW loading may also due to the uniform dispersion of CHNW and the high cross-link density (Domini, Joseph, Sabura Begum et al., 2020). The value of the storage modulus is an indication of stiffness and cross-link density of composites (Cao et al., 2013). The values of storage modulus are in line with the cross-link density measurement of the composites reported under swelling studies. At 6 phr CHNW loading, filler-filler interaction over ways matrix-filler interactions and the agglomeration between the whiskers (evident from the SEM analysis of the composite, Fig. 5) results in low cross-link density owing to decrease in storage modulus.

The loss modulus (E'') is a measure of energy lost to friction as heat in NBR-CHNW composites. The loss modulus values of NBR nanocomposites were found to be higher than that of virgin NBR. The loss modulus peaks of NBR nanocomposites were broader than NBR gum owing to the increased energy absorption of chitin nanowhiskers (Pongdong, Nakason, Kummerlöwe, & Vennemann, 2015). The increase in the magnitude of E'' of the prepared nanocomposites is might be due to the energy dissipation that arises from a breakdown of CHNW transient networks and loss of trapped rubber chains on the filler surface during dynamic tests (Prasertsri & Rattanasom, 2012). From the maxima of the loss modulus curve (E'' vs. T), the glass transition temperature (T_g) of the composites was determined. The T_g of NBR, NBR-CHNW2, NBR-CHNW6 was found to be −11.15 °C, −8.90 °C, and −9.68 °C respectively. The DMA results showed that T_g values were increased by the addition of CHNW to the NBR matrix and the maximum value was reported for 2 phr CHNW addition. The positive shift in the glass transition temperature of NBR-CHNW nanocomposites was clear evidence of effective interfacial interaction between the matrix and the filler (Chen, Peng, Kong, Huang, & Li, 2008).

The loss tangent (tan δ) is the ratio of loss modulus (E'') and storage modulus (E'). It is a parameter to determine the mechanical damping and the internal friction in the prepared NBR-CHNW composites (Dominic, Joseph, Begum et al., 2020). The temperature at which the maximum tan δ peak is considered as the glass transition temperature of the prepared composites (Dileep, Varghese, Sivakumar, & Narayanankutty, 2019). It was observed that the addition of CHNW into the NBR matrix, decreases the loss tangent peak height and shifts the maximum tan δ peak to a higher temperature region. The magnitude of the maximum tan δ ($tan\delta_{max}$) value of NBR, NBR-CHNW2, NBR-CHNW6 was found to be 1.535, 0.985, 1.119 respectively. Balachandran et al. reported similar findings when nano-calcium carbonate is used as a reinforcing filler in NBR (Balachandran & Bhagawan, 2012). The decrease in tanδ peak height in NBR-CHNW composites is clear evidence of the hindering of rubber molecular chains by CHNW and improved interfacial interaction (Joseph et al., 2010). The homogenous dispersion of CHNW at 2 phr loading in the NBR matrix results in more constrained polymer domains around the surface of incorporated chitin nanowhiskers compared to NBR-CHNW6 composite. This might be the reason for the low value of $tan\delta_{max}$ in NBR-CHNW2 composite

Table 4
DMA data of NBR and NBR-CHNW nanocomposites.

Properties	NBR	NBR–CHNW2	NBR–CHNW6
T_g (according to tanδ max)(°C)	−4.09	2.78	1.07
T_g (according to E" max) (°C)	−11.15	−8.90	−9.68
Tanδ maximum	1.535	0.985	1.119
Storage modulus (MPa) at 25 °C	3.651	6.157	5.968
Storage modulus (MPa) at −40 °C	1189	1473	1384
Volume fraction of immobilized polymer chain, (C_v)	–	0.0875	0.0601
Adhesion factor, A	–	−0.3449	−0.2244

compared to NBR-CHNW6. The Tg according to maximum tan δ of NBR gum, NBR-CHNW2, NBR-CHNW6 composite was found to be −4.09 °C, 2.78 °C and 1.07 °C respectively. Yukun Chen et. al reported a positive shift in T_g from −1.78 °C to 1.34 °C by the incorporation of 15 phr nanocrystalline cellulose in NBR foam (Chen et al., 2015). The significant improvement in T_g of NBR-CHNW composites showed the reinforcing action of CHNW (Dominic, Joseph, Begum et al., 2020).

The mechanical properties of NBR-CHNW composites were greatly influenced by the constrained region. The volume fraction of immobilized polymer chain (C_v) and adhesion parameter (A) of NBR-CHNW composites were determined according to the procedure given by Formela et al. (2016). The C_v values of NBR-CHNW2 and NBR-CHNW6 composites were found to be 0.0875 and 0.0601 respectively. The high C_v value of NBR-CHW2 composite compared to NBR-CHN6 showed the effective immobilization of polymer chains at 2 phr CHNW loading. The 'A' value of NBR-CHNW2 and NBR-CHNW6 composites were found to be −0.3449 and −0.2244 respectively. Lower the value of 'A' more will be the interfacial addition and enhanced interaction between CHNW and NBR (Formela et al., 2016). The more negative value of 'A' obtained for NBR-CHNW2 composite showed better reinforcing action of chitin nanowhiskers at 2 phr, which is in line with the mechanical and swelling studies results. Thus it was possible to observe that CHNW reinforced NBR composites showed better dynamic properties than NBR gum and these nanowhiskers decreases the damping of the composites significantly. The DMA analysis data was summarised in Table 4.

4. Conclusion

With the evolution and progress of green and sustainable nanofillers, rubber technology has been undergoing change. Novel nanomaterials are replacing conventional fillers to improve the performance of the general-purpose and specialty rubbers significantly at lower loadings. The present work has been undertaken in this context to develop acrylonitrile-butadiene rubber (NBR)-chitin nanowhisker (CHNW) composite to upgrade the processing and performance properties of NBR. Chitin nanowhiskers (CHNW) were synthesized from shrimp shells by employing the demineralization, bleaching, acid hydrolysis techniques followed by homogenization. The synthesized chitin nanowhiskers were characterized using different analytical techniques like FTIR, XRD, TEM, TGA etc. The FTIR analysis and XRD pattern of CHNW show that α chitin is present in the synthesized sample. The crystallinity index of CHNW was found to be 86 %. The formation and morphology of CHNW were confirmed by TEM analysis and the aspect ratio of the whiskers was in the range 12−16. Thermogravimetric analysis shows that thermal degradation of chitin takes place in a single step and the temperature at which 50 % degradation occurs was found to be at 335 °C.

Chitin nanowhisker (CHNW) reinforced NBR composites were prepared using a masterbatch of CHNW in NBR latex followed by dry rubber compounding in a two roll mills. The cure characteristics, mechanical, technological, thermal, swelling and dynamic mechanical properties were analyzed. Cure rate index decreased by the incorporation of CHNW in the NBR matrix. The tensile strength and tear strength of NBR-CHNW2 composites showed an improvement of 116 % and 54 % respectively compared to neat NBR. The improvement in the tensile modulus and cross-link density of NBR-CHNW composites can be attributed to the 'caged' or 'trapped' rubber chains in the three-dimensional rigid hydrogen-bonded network of chitin nanowhiskers. The swelling index of NBR-CHNW2 composite was found to be less than that of NBR gum. The fractographic studies of NBR-CHNW composites revealed effective stress transfer in the composite. The NBR-CHNW composites showed an ample improvement in the onset degradation temperature (T_{on}), the temperature at which 50 % degradation occurs (T_{50}). The DMA studies revealed that the glass transition temperature of NBR-CHNW2 composite is about 6 °C more than that of neat NBR. The lowering of tan δ peak height in NBR-CHNW composites shows the effective interaction of CHNW with NBR matrix. Based on the presented results, it can be concluded that chitin nanowhiskers seem to be promising green filler for NBR for high performance elastomeric applications.

CRediT authorship contribution statement

Midhun Dominic C.D.: Conceptualization, Methodology, Visualization, Writing - original draft. **Rani Joseph:** Supervision. **P.M. Sabura Begum:** Supervision. **Aswathy Raghunandanan:** Data curation, Resources. **Nelwin T. Vackkachan:** Investigation. **Dileep Padmanabhan:** Data curation, Resources. **Krzysztof Formela:** Writing - review & editing.

Declaration of Competing Interest

The authors declare no conflicts of interest.

Acknowledgment

The authors greatly acknowledge SAIF STIC, CUSAT for chemical analysis and J J Murphy Research Centre, Kerala for rubber compounding.

References

Abdul Rashid, E. S., Muhd Julkapli, N. B., & Abdul Hadi Yehya, W. (2018). Reinforcement effect of nanocellulose on thermal stability of nitrile butadiene rubber (NBR) composites. *Journal of Applied Polymer Science, 135*(32), 46594.

Aklog, Y. F., Nagae, T., Izawa, H., Morimoto, M., Saimoto, H., & Ifuku, S. (2016). Preparation of chitin nanofibers by surface esterification of chitin with maleic anhydride and mechanical treatment. *Carbohydrate Polymers, 153*, 55–59.

Alvarez, F. J. (2014). The Effect of chitin size, shape, source and purification method on immune recognition. *Molecules, 19*(4), 4433–4451.

Azman Mohammad Taib, M. N., Yeheye, W., & Muhd Julkapli, N. (2020). Synthesis and characterization of nanocrystalline cellulose as reinforcement in nitrile butadiene rubber composites. *Cellulose Chemistry and Technology, 54*(1), 11–25.

Balachandran, M., & Bhagawan, S. S. (2012). Mechanical, thermal and transport properties of nitrile rubber (NBR)-nanoclay composites. *Journal of Polymer Research, 19*(2), 9809.

Biradar, B., Maladkar, K., & Kittur, A. A. (2016). Extraction of chitin from prawn shell and preparation of chitosan. *Research Journal of Chemical and Environmnetal Sciences, 4*, 70–73.

Bo, M., Bavestrello, G., Kurek, D., Paasch, S., Brunner, E., Born, R., ... Ehrlich, H. (2012). Isolation and identification of chitin in the black coral Parantipathes larix (Anthozoa: Cnidaria). *International Journal of Biological Macromolecules, 51*(1–2), 129–137.

Boonbumrung, A., Sae-oui, P., & Sirisinha, C. (2016). Reinforcement of multiwalled carbon nanotube in nitrile rubber: In comparison with carbon black, conductive carbon black, and precipitated silica. *Journal of Nanomaterials, 2016*, 1–8.

Boonstra, W. J., Valman, M., & Björkvik, E. (2018). A sea of many colours – How relevant is Blue Growth for capture fisheries in the Global North, and vice versa? *Marine Policy, 87*(September 2017), 340–349.

Bryan, E., & Welding, G. N. (1964). Ellis and Freud.pdf. *Rubber Chemistry and Technology, 37*(2), 571–575.

Cao, X., Xu, C., Wang, Y., Liu, Y., Liu, Y., & Chen, Y. (2013). New nanocomposite materials reinforced with cellulose nanocrystals in nitrile rubber. *Polymer Testing, 32*(5), 819–826.

Chen, Y., Peng, Z., Kong, L. X., Huang, M. F., & Li, P. W. (2008). Natural rubber nanocomposite reinforced with nano silica. *Polymer Engineering and Science, 48*(9),

1674–1677.
Chen, Y., Zhang, Y., Xu, C., & Cao, X. (2015). Cellulose nanocrystals reinforced foamed nitrile rubber nanocomposites. *Carbohydrate Polymers, 130*, 149–154.
De, D., Kr. Panda, P., Roy, M., Bhunia, S., & Ismail Jaman, A. (2012). Reinforcing effect of nanosilica on the properties of natural rubber/reclaimed ground rubber tire vulcanizates. *Polymer Engineering and Science, 53*, 227–237.
Dileep, P., Varghese, G. A., Sivakumar, S., & Narayanankutty, S. K. (2019). An innovative approach to utilize waste silica fume from zirconia industry to prepare high performance natural rubber composites for multi-functional applications. *Polymer Testing, 81*(January), 106172.
Dominic, M., Joseph, R., Sabura Begum, P. M., Kanoth, B. P., Chandra, J., & Thomas, S. (2020). Green tire technology: Effect of rice husk derived nanocellulose (RHNC) in replacing carbon black (CB) in natural rubber (NR) compounding. *Carbohydrate Polymers, 230*(February), 115620.
Dominic, C. D. M., Joseph, R., Begum, P. M. S., Joseph, M., Padmanabhan, D., Morris, L. A., ... Formela, K. (2020). Cellulose nanofibers isolated from the Cuscuta reflexa plant as a green reinforcement of natural rubber. *Polymers, 12*(4), 814.
Ekblad Alf, S. T. (1996). Determination of chitin in fungi and mycorrhizal roots by an improved HPLC analysis of glucosamine. *Plant and Soil, 178*(1), 29–35.
Eyssa, H. M., Abulyazied, D. E., Abdulrahman, M., & Youssef, H. A. (2017). Mechanical and physical properties of nanosilica/nitrile butadiene rubber composites cured by gamma irradiation. *Egyptian Journal of Petroleum, 2017*, 1–10.
Eyssa, H. M., Abulyazied, D. E., Abdulrahman, M., & Youssef, H. A. (2018). Mechanical and physical properties of nanosilica/nitrile butadiene rubber composites cured by gamma irradiation. *Egyptian Journal of Petroleum, 27*(3), 383–392.
Fan, Y., Saito, T., & Isogai, A. (2008). Chitin nanocrystals prepared by TEMPO-mediated oxidation of α-chitin. *Biomacromolecules, 9*(1), 192–198.
Fazli, A., & Rodrigue, D. (2020). Waste rubber recycling: A review on the evolution and properties of thermoplastic elastomers. *Materials, 13*(3), 782.
Flory, P. J., & Rehner, J. (1943). Statistical mechanics of crosslinked polymer networks I. Rubberlike elasticity. *The Journal of Chemical Physics, 11*(1), 512–520.
Formela, K., Hejna, A., Piszczyk, Ł., Saeb, M. R., & Colom, X. (2016). Processing and structure–property relationships of natural rubber/wheat bran biocomposites. *Cellulose, 23*(5), 3157–3175.
Garrido, T., Etxabide, A., de la Caba, K., & Guerrero, P. (2017). Versatile soy protein films and hydrogels by the incorporation of β-chitin from squid pens (*Loligo* sp.). *Green Chemistry, 19*(24), 5923–5931.
Gopalan Nair, K., & Dufresne, A. (2003). Crab shell chitin whisker reinforced natural rubber. *Biomacromolecules, 4*(3), 657–665.
Hu, X., Zhao, H., Li, T., He, X., Wang, X., Pellerin, C., ... Zhang, R. (2020). Acrylonitrile–butadiene rubber reinforced by graphene oxide/halloysite nanotubes hybrid nanofillers through mechanical blending method. *Plastics Rubber and Composites, 49*(4), 141–149.
Jang, M. K., Kong, B. G., Jeong, Y., Il, Lee, C. H., & Nah, J. W. (2004). Physicochemical characterization of α-chitin, β-chitin, and γ-chitin separated from natural resources. *Journal of Polymer Science Part A: Polymer Chemistry, 42*(14), 3423–3432.
Joseph, S., Appukuttan, S. P., Kenny, J. M., Puglia, D., Thomas, S., & Joseph, K. (2010). Dynamic mechanical properties of oil palm microfibril-reinforced natural rubber composites. *Journal of Applied Polymer Science, 117*(3), 1298–1308.
Kader, M. A., Kim, K., Lee, Y. S., & Nah, C. (2006). Preparation and properties of nitrile rubber/montmorillonite nanocomposites via latex blending. *Journal of Materials Science, 41*(22), 7341–7352.
Kadokawa, J. I., Takegawa, A., Mine, S., & Prasad, K. (2011). Preparation of chitin nanowhiskers using an ionic liquid and their composite materials with poly(vinyl alcohol). *Carbohydrate Polymers, 84*(4), 1408–1412.
Kaya, M., Seyyar, O., Baran, T., & Turkes, T. (2014). Bat guano as new and attractive chitin and chitosan source. *Frontiers in Zoology, 11*(1), 1–10.
Li, M.-C., Zhang, Y., & Cho, U. R. (2014). Mechanical, thermal and friction properties of rice bran carbon/nitrile rubber composites: Influence of particle size and loading. *Materials & Design, 63*, 565–574.
Liu, Y., Liu, M., Yang, S., Luo, B., & Zhou, C. (2018). Liquid crystalline behaviors of chitin nanocrystals and their reinforcing effect on natural rubber. *ACS Sustainable Chemistry & Engineering, 6*(1), 325–336.
Lu, Y., Weng, L., & Zhang, L. (2004). Morphology and properties of soy protein isolate thermoplastics reinforced with chitin whiskers. *Biomacromolecules, 5*(3), 1046–1051.
Maria, A., De Sousa, F., Cesar, A., Peres, D. C., Russi, C., Furtado, G., ... Visconte, Y. (2017). Mixing process influence on thermal and rheological properties of NBR/SiO2 from rice husk ash. *Polimeros, 27*(2), 93–99.
Mincea, M., Negrulescu, A., & Ostafe, V. (2012). Preparation, modification, and applications of chitin nanowhiskers: A review. *Review on Advanced Material Science, 30*, 225–242.
Nge, T. T., Hori, N., Takemura, A., Ono, H., & Kimura, T. (2003). Phase behavior of liquid crystalline chitin/acrylic acid liquid mixture. *Langmuir, 19*(4), 1390–1395.
Ofem, M. I., Anyandi, A. J., & Ene, E. B. (2017). Properties of chitin reinforces composites: A review. *Nigerian Journal of Technology, 36*(1), 57–71.
Pillai, C. K. S., & Sharma, C. P. (2009). Electrospinning of chitin and chitosan nanofibres. *Trends in Biomaterials & Artificial Organs, 22*(3), 179–201.
Pongdong, W., Nakason, C., Kummerlöwe, C., & Vennemann, N. (2015). Influence of filler from a renewable resource and silane coupling agent on the properties of epoxidized natural rubber vulcanizates. *Journal of Chemistry, 2015*(January), 1–15.
Prasanth Kumar, R., Getthakumari Amma, M., & Sabu, T. (1995). Short sisal fiber reinforced styrene butadiene rubber composites. *Journal of Applied Polymer Science, 58*(3), 597–612.
Prasertsri, S., & Rattanasom, N. (2012). Fumed and precipitated silica reinforced natural rubber composites prepared from latex system: Mechanical and dynamic properties. *Polymer Testing, 31*(5), 593–605.
Rattanasom, N., Saowapark, T., & Deeprasertkul, C. (2007). ARTICLE IN PRESS POLYMER Reinforcement of natural rubber with silica/carbon black hybrid filler. *Polymer Testing, 26*, 369–377.
Ravi Kumar, M. N. V. (2000). A review of chitin and chitosan applications. *Reactive & Functional Polymers, 46*(1), 1–27.
Sadeghalvaad, M., Dabiri, E., Zahmatkesh, S., & Afsharimoghadam, P. (2019). Improved curing conditions and mechanical/chemical properties of nitrile butadiene rubber composites reinforced with carbon based nanofillers. *Journal of Nanostructures, 9*(3), 453–467.
Sae-Oui, P., Rakdee, C., & Thanmathorn, P. (2002). Use of rice husk ash as filler in natural rubber vulcanizates: In comparison with other commercial fillers. *Journal of Applied Polymer Science, 83*(11), 2485–2493.
Salkhord, S., & Sadeghi Ghari, H. (2015). Synergistic reinforcement of NBR by hybrid filler system including organoclay and nano-CaCO3. *Journal of Applied Polymer Science, 132*(44), 1–14.
Sini, T. K., Santhosh, S., & Mathew, P. T. (2007). Study on the production of chitin and chitosan from shrimp shell by using Bacillus subtilis fermentation. *Carbohydrate Research, 342*(16), 2423–2429.
Tang, Q. Y., & Zhang, W. F. (2014). Environmental factors on aging of nitrile butadiene rubber (NBR)—A review. *Advanced Materials Research, 1033–1034*, 987–990.
Tian, M., Su, L., Cai, W., Yin, S., Chen, Q., Fong, H., ... Zhang, L. (2011). Mechanical properties and reinforcement mechanisms of hydrogenated acrylonitrile butadiene rubber composites containing fibrillar silicate nanofibers and short aramid microfibers. *Journal of Applied Polymer Science, 120*, 1399–1447.
Villa-Lerma, G., González-Márquez, H., Gimeno, M., López-Luna, A., Bárzana, E., & Shirai, K. (2013). Ultrasonication and steam-explosion as chitin pretreatments for chitin oligosaccharide production by chitinases of Lecanicillium lecanii. *Bioresource Technology, 146*, 794–798.
Visakh, P. M., Monti, M., Puglia, D., Rallini, M., Santulli, C., Sarasini, F., ... Kenny, J. M. (2012). Mechanical and thermal properties of crab chitin reinforced carboxylated SBR composites. *Express Polymer Letters, 6*(5), 396–409.
Visakh, P. M., Thomas, S., Oksman, K., & Mathew, A. P. (2012). Crosslinked natural rubber nanocomposites reinforced with cellulose whiskers isolated from bamboo waste: Processing and mechanical/thermal properties. *Composites Part A: Applied Science and Manufacturing, 43*(4), 735–741.
Wysokowski, M., Motylenko, M., Bazhenov, V. V., Stawski, D., Petrenko, I., Ehrlich, A., ... Ehrlich, H. (2013). Poriferan chitin as a template for hydrothermal zirconia deposition. *Frontiers of Materials Science, 7*(3), 248–260.
Yu, P., He, H., Luo, Y., Jia, D., & Dufresne, A. (2017). Elastomer reinforced with regenerated chitin from alkaline/urea aqueous system. *ACS Applied Materials & Interfaces, 9*(31), 26460–26467.
Zhang, X., & Rolandi, M. (2017). Engineering strategies for chitin nanofibers. *Journal of Materials Chemistry B: Materials for Biology and Medicine, 5*(14), 2547–2559.
Zhang, C., Dan, Y., Peng, J., Turng, L.-S., Sabo, R., & Clemons, C. (2014). Thermal and mechanical properties of natural rubber composites reinforced with cellulose nanocrystals from southern pine. *Advances in Polymer Technology, 33*(S1), 1–7.
Zhang, Z., He, X., Wang, X., Rodrigues, A. M., & Zhang, R. (2018). Reinforcement of the mechanical properties in nitrile rubber by adding graphene oxide/silicon dioxide hybrid nanoparticles. *Journal of Applied Polymer Science, 135*(14), 46091.
Zhong, R., Zhang, Z., Zhao, H., He, X., Wang, X., & Zhang, R. (2018). Improving thermo-oxidative stability of nitrile rubber composites by functional graphene oxide. *Materials, 11*(6), 921.